Research Article

Sansabilla Bouchareb*, Rachid Tigrine, and Sabah Fetah

Vibrational wave scattering in disordered ultra-thin film with integrated nanostructures

https://doi.org/10.1515/arh-2022-0135
received November 23, 2022; accepted December 29, 2022

Abstract: A theoretical model, the phase-field matching theory, has been used to investigate the localized states, their associated states, the local vibrational density of states, the coherent conductance, and the associated thermal conductivity of the perturbed ultra-thin film quasi-dimensional crystalline lattice. The defect disrupts the system's translational symmetry in the perpendicular direction to it, which is axis Ox, and induces a localized state in its behavior that is not present in the bulk, scattering the incident elastic wave. The model was analyzed for three different cases of elastic parameters: softening, homogeneous, and hardening. The purpose is to investigate how the local dynamics can respond to changes in the microscopic environment in the perturbed domain. The analysis of the total phononic conductance spectra and the local vibrational densities states identifies distinguishing characteristics and demonstrates the sensor's potential use in nondestroyed control.

Keywords: localized state, thin film, transmission and reflection, density of states, Landauer–Büttiker, formalism, PMFT

1 Introduction

One of the major trends in contemporary science and technology is the race for miniaturization. Several materials are increasingly being developed at the nanoscopic scale, with the aim of integrating them into mesoscopic physical devices. In these devices, the material components have a surface area relative to their mass that is greater, in the broad sense, than in conventional devices of larger size. This can, in fact, influence their physical properties. On the other hand, the so-called quantum effects may begin to dominate the behavior of these nanometer-scale components and thereby alter their physical properties such as electrical, magnetic, optical, and other properties.

In these new low-dimensional nanostructures with variable and complex geometries, the elementary excitations could thus be subjected to confinement and to quantum and coherent behavior.

The material development of nanostructures is done mainly by the "top-down" technique. This kind of technique consists of producing very small structures by chemical attack starting from large pieces. Nanostructures can also be obtained by "bottom-up" techniques by manipulating and depositing, atom by atom, or molecule by molecule, materials in a required geometry. This mastery of new techniques now makes it possible to obtain well-controlled nanoscale objects. The characterization and the experimental study of these nanostructures are carried out by a wide range of techniques; two of the main techniques are the scanning tunneling microscope and the atomic force microscope. Historically, most works in this field of coherent transport have been directed toward the study of electronic properties in waveguides containing nanostructures. One of the most privileged and most used formalisms was that of Landauer and Büttiker [1,2]. However, the coherent transport properties of phonons and magnons in low-dimensional systems and in waveguides containing nanostructures are less studied experimentally and theoretically. This is despite their importance for understanding certain physical effects such as heat exchange for mesoscopic devices and surface adsorption and catalysis. Nevertheless, increasing interest has been given in recent years to the properties of phonons and magnons in nanoscopic systems. In a material, the atoms of a solid are generally placed on a crystal lattice. These atoms are not fixed but perform movements and oscillations,

* **Corresponding author: Sansabilla Bouchareb,** Département Sciences de la matière, Laboratoire, d'énergie, Environnement et Systèmes d'informations, Université Ahmed Draya Adrar, Adrar, Algérie, e-mail: sansabilla123@gmail.com
Rachid Tigrine: Département Sciences de la matière, Laboratoire, d'énergie, Environnement et Systèmes d'informations, Université Ahmed Draya Adrar, Adrar, Algérie; Laboratoire, De Physique et Chimie Quantiques, Université Mouloud Memmeri Tizi Ouzou, Tizi Ouzou, Algérie
Sabah Fetah: Département de Physique, Faculté des Sciences, Université de M'sila, M'Sila, Algérie

depending on thermal agitation, around their position of equilibrium [3]. The long-range order in these solids allows local oscillations to propagate like elastic waves through the system. The energies of these waves are generally dispersive [4]. Wave propagation in low-dimensional systems is strongly disrupted by the presence of various types of inhomogeneities, which causes changes in physical properties such as the induction of localized states in the vicinity of each defect, thereby modifying the system's conductance [5–8].

In this article, the theoretical description of the system and the vibrational dynamics was presented in the bulk. The essentials of the method used to carry out our research work for the determination of the states located in the neighborhood of the implanted defects were given. Green's formalism was recalled for the determination of the density of state (DOS) associated with these localized states induced by the defect. The scattering of elastic waves and the theoretical method of Landauer–Büttiker for the calculation of the transmission and reflection coefficients as well as the phononic conductance were presented. The thermal conductivity associated with phonons was calculated.

2 Theoretical description of the model and the vibrational dynamics at the bulk

The studied model is a quasi-one-dimensional waveguide, which is typically modeled structurally as a very thin layer with one, two, or three implanted chains of foreign atoms, as shown in Figure 1a–d. This system is assumed to be free of surface elastic constants. By applying the equation of motion to bulk sites, a homogeneous system of the form was obtained:

$$[\Omega^2 I - D(\overrightarrow{q}, r_2, \text{expi}\varphi_x, \text{expi}\varphi_y)]|u\rangle = |0\rangle, \tag{1}$$

where $D(\overrightarrow{q}, r_2)$ are the dynamic matrix $(2N \times 2N)$ and $|u\rangle$ is the displacement vector of the atoms of the elementary cell.

To satisfy the condition $|u\rangle \neq |0\rangle$, the system (1) must check the following compatibility conditions:

$$\text{Det}[\Omega^2 I - D(\overrightarrow{q}, r_2)] = 0. \tag{2}$$

We thus obtain, for each mode, $(\overrightarrow{q}, \Omega)$ solutions such $|Z| \leq 1$ as characterizing the various vibration waves propagating in the direction Oy parallel to the defect.

Equation (2) admits complex or real roots in pairs Z and Z^{-1}, which must be sorted according to the following physical considerations: Let us start Z with the complex of norm 1. The wave vectors are, in this case, real and the couples, and the number of propagating vibrations was found. The direction of propagation is given by the sign of the group speed. Thanks to the parity of the dispersion relations, we can choose at each frequency of each branch a wave propagating from left to right. For Z reals or complex, whose norm is different from 1, the criterion of choice between the two terms of the pair Z and Z^{-1} is less arbitrary. Indeed, one of the solutions corresponds to an attenuated wave, while the other mode diverges depending on the position of the atom. Physics obviously requires considering only the attenuated modes identified by the condition $|Z| < 1$. Conversely, the propagating modes transporting energy are characterized by $|Z| = 1$. In Figures 1–4, the relationships between dispersion in bulk as a function of the angle of incidence phix, the absolute value of the phase factors 2D and 3D as a function of the ratio of the elastic constants in volume between first and second neighbors, and finally, the group velocities of the propagating mode 1 and mode 2 are presented [9–15].

3 Scattering via the defect

To investigate the scattering phenomenon, we need the defect matrix and the matching matrix, as well as the incident vector. We first determine that the defect matrix originates from the writing of the equations of motion of the atoms that describe the inhomogeneity (Figure 1a–c). This study region is chosen such that it includes the perturbed region as well as atoms of the matching region and possesses a perfect waveguide environment. The matrix corresponding to the writing of the equations of motion of these atoms is a rectangular one, which can then be written in the following form:

$$Md|u\rangle = 0. \tag{3}$$

Within the framework of our modeling, the goal of this section is to establish a relationship between the vibrational displacements of the atoms in the perturbed domain and the phase factor fields induced by the study of the two perfect waveguides. The atomic displacements of the sites belonging to the matching region are represented by a linear combination, defining a finite space. In this case, there are two matching regions on the left and right of the defect, so we need to define two bases and two functions, the first being for the matching region on

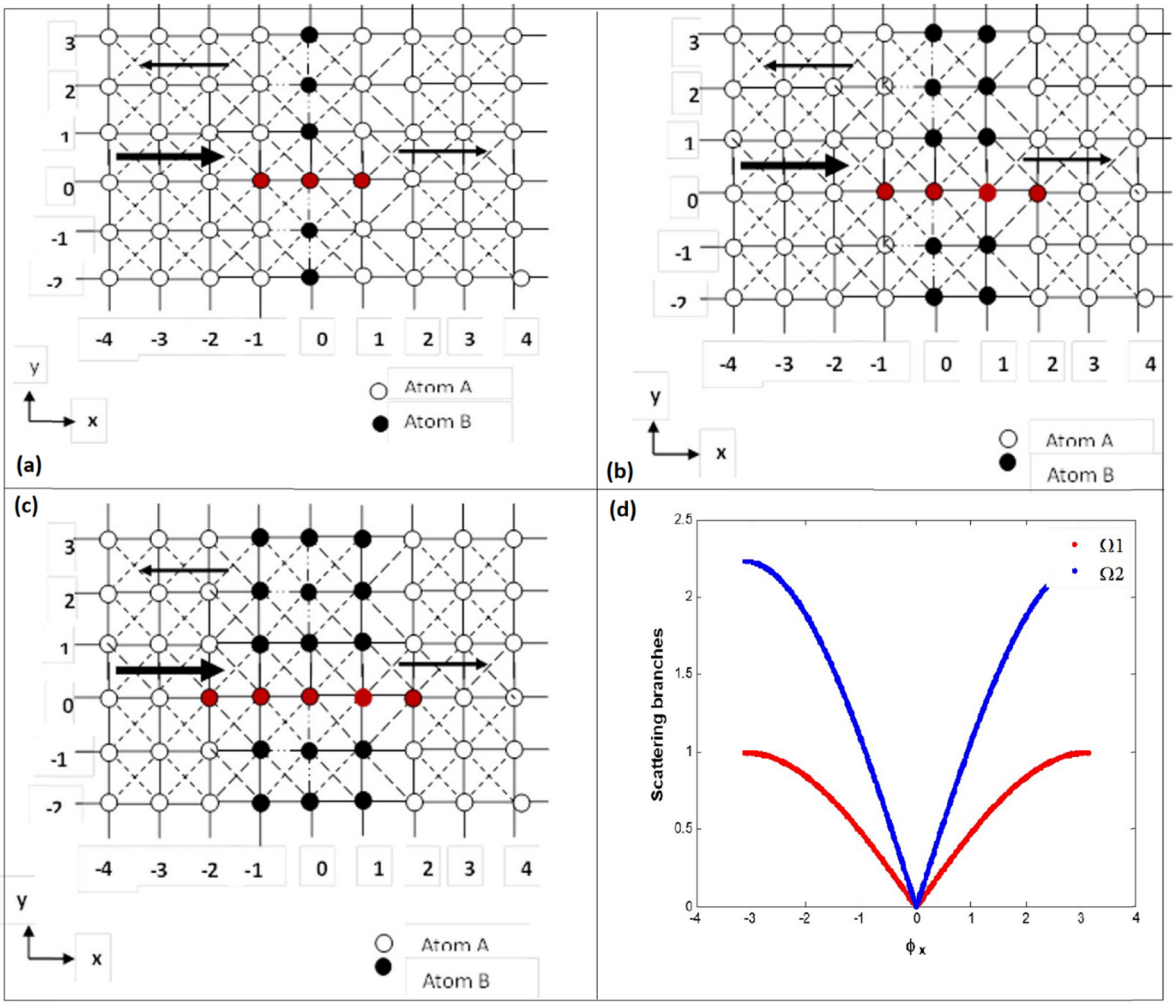

Figure 1: (a) System with one integrated chain. (b) System model with two integrated chains. (c) System model with three integrated chains. (d) Dispersion branches of mode 1 and mode 2 as function ϕ_x and $r2$ ration of elastic constant of first and second neighbors.

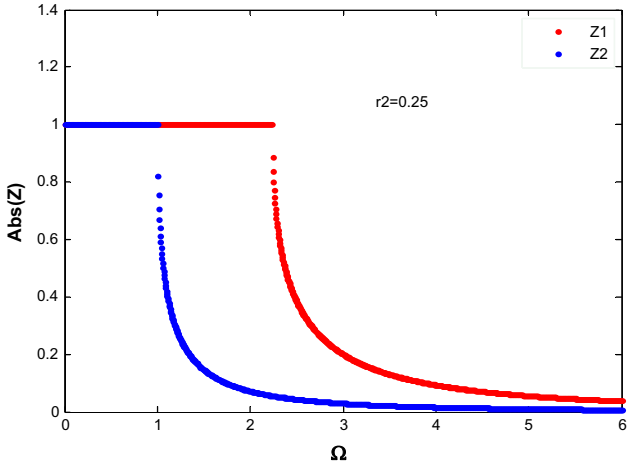

Figure 2: Absoluteof phase factor Z as function, $r2$ and dimensionless frequency Ω.

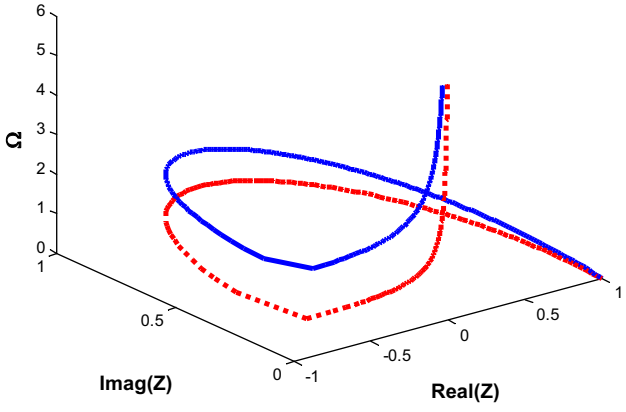

Figure 3: Representation 3D of phase factor as function $r2$ (image Z and real Z).

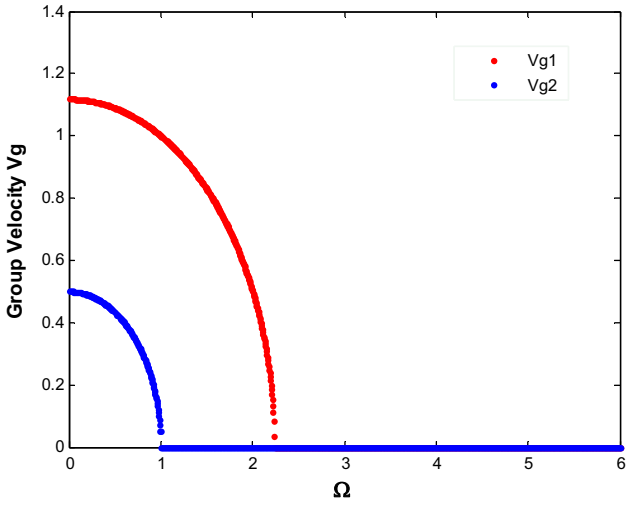

Figure 4: Group velocity mode 1 and mode 2 as function *r*2 and dimensionless frequencies Ω.

the left side of the atomic quasi-two-dimensional defect system and the second for the right side of the system. The dimensions of the unit vectors are related to the number of the eigenvalues and the eigenvectors obtained by the vibrational dynamic study of the two perfect waveguides.

Consider the case of a propagating incident mode, coming from the left perfect waveguide and going toward the right perfect waveguide, as shown in Figure 1a–c. The resulting wave scattered by the defect zone breaks down into two parts: one is transmitted and the other is reflected, which gives rise to a vibrational field of displacement in the two half-spaces that must be developed on the basis of the eigenmodes and the eigenvectors induced from the dynamic study of the bulk. The Cartesian component of the displacement field of an atom outside the defect region can be expressed using the matching method. The atomic displacements in the two Cartesian directions of an atomic site belonging to the left perfect waveguide can be expressed as the superposition of the incident wave with the eigenmodes of vibration of the left perfect waveguide at the same frequency [7,8,16–28].

$$u'_{\alpha}(n_x, n_y) = u(\alpha, v')\cdot Z_{v'}^{nx} + \sum_{v'}(Z_{v'})^{-nx}\cdot R\cdot u(\alpha, v') \text{ with } n_x < -2. \quad (4)$$

In the same way, for an atomic site of the perfect right waveguide, the atomic displacements can be expressed as follows:

$$u_{\alpha}(n_x, n_y) = \sum_{v'}(Z_{v'})^{nx}\cdot T\cdot u(\alpha, v') \text{ with } n_x > 2. \quad (5)$$

The quantity R, as we will see later, is related to the reflection coefficients of an incident mode v according to the eigenmodes $v'$of the left perfect waveguide for a given frequency. Likewise, T is the quantity associated with the transmission coefficients of the incident mode $v$according to the eigenmodes v' of the right waveguide. The physical quantities $u(\alpha, v)$ and $u(\alpha, v')$ represent the atomic displacement of the sites at the two perfect half-spaces, respectively, at the left and right of the defect, and they are determined using the eigenvectors of the dynamic matrices of the two perfect waveguides.

The transmission and reflection coefficients are calculated for a propagating mode, knowing that describes modes, which can be propagating or evanescent in the domain frequencies for mode 1 $\Omega_1 = [0, 1]$ and for mode 2 $\Omega_2 = [0, 2.4]$.

The vector of atomic displacements of the sites of the elementary cell of the zones of defect and of matching region can be broken down into two parts:

The first part is constituted of the displacements of the irreducible sites forming the defect region. The second part constituted of matching sites. Let $\{R\}$ and $\{T\}$ be the two bases, and we will thus have:

$$|u\rangle = \begin{pmatrix} |irr\rangle \\ |rac\rangle \end{pmatrix}. \quad (6)$$

We can then describe the connection of atoms using the following expression:

$$|u\rangle = \begin{pmatrix} |irr\rangle \\ |rac\rangle \end{pmatrix} = [Mr]\begin{pmatrix} |irr\rangle \\ |RT\rangle \end{pmatrix} + |IH\rangle. \quad (7)$$

We multiply system (7) by the defect matrix Md and we end up with system 2.

$$[Md]\cdot|u\rangle = [Md]\cdot\begin{pmatrix} irr \\ rac \end{pmatrix} = [Md]\cdot[Mr]\cdot\begin{pmatrix} |irr\rangle \\ |RT\rangle \end{pmatrix} + [Md]\cdot|IH\rangle. \quad (8)$$

This can be summed up as follows:

$$[Md]\cdot[Mr]\cdot\begin{pmatrix} |irr\rangle \\ |RT\rangle \end{pmatrix} = [Mp]\cdot\begin{pmatrix} |irr\rangle \\ |RT\rangle \end{pmatrix} = -[Mp]\cdot|IH\rangle, \quad (9)$$

and we deduce that

$$\begin{pmatrix} |irr\rangle \\ |RT\rangle \end{pmatrix} = -[Mp]^{-1}\cdot[Md]\cdot|IH\rangle. \quad (10)$$

System (10) allows me to calculate the transmission and reflection coefficients and, subsequently, the phononic conductance. The reflection and transmission coefficients can then be calculated by normalizing them using group speeds, which conserve energy and give the sum of the reflected and transmitted parts equal to 1. For waves coming from the left side of the defect according to the eigenmodes, the reflection coefficient is given by:

$$r_{vv'} = \left(\frac{vg_{v'}}{vg_v}\right)|R|^2. \tag{11}$$

The transmission coefficient is given by:

$$t_{vv'} = \left(\frac{vg_{v'}}{vg_v}\right)|T|^2, \tag{12}$$

where vg_v is the mode and v is the group speed and vanishes for the evanescent modes of the two perfect waveguides. Indeed, evanescent modes are necessary for a full description of vibrational dynamics and for the diffusion of phonons in crystallographic waveguides although they do not contribute to energy transport. Then the transmittance of the system is defined by the following relation:

$$\sigma_v = \sum_{v'} t_{vv'}. \tag{13}$$

The coefficients of transmission and reflections are represented by the curves shown in Figures 5–10.

In addition, the phononic transmittance is presented in Figure 11 as function dimensionless Ω and elastic constant of the perturbed system [29–33].

4 Heat transport by multichannel system

The thermal conductivity of a system reflects the ability of a material to transmit heat by conduction. At the atomic scale, heat transfer in solids can be accomplished through any particle or quasi-particle. Thermal conductivity is the sum of the contributions of each particle or quasi-particle. In solids, heat transfer is mainly due to phonons, electrons, and magnons. Phonons can represent an important part of the thermal conductivity in certain materials such

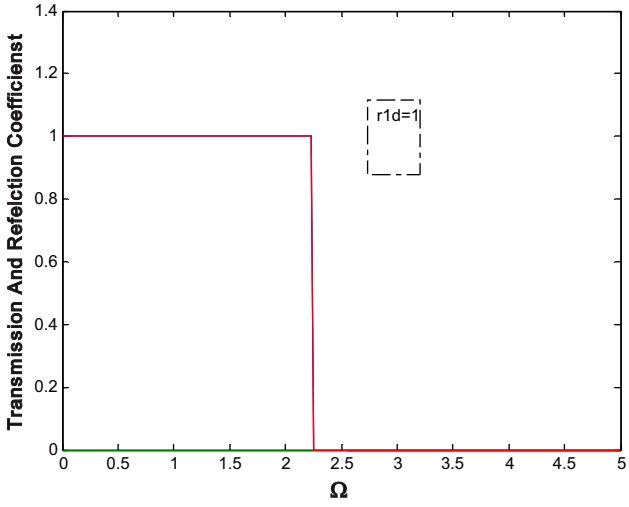

Figure 6: Transmission and reflection coefficients in the case of homogeneous mode 1.

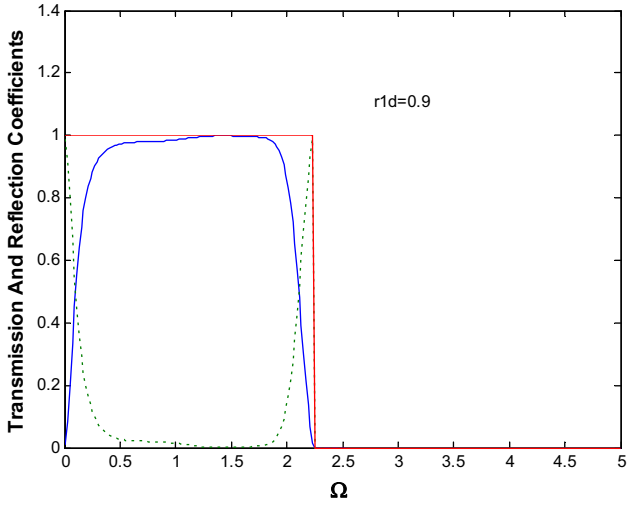

Figure 5: Transmission and reflection coefficients in the case of softening mode 1.

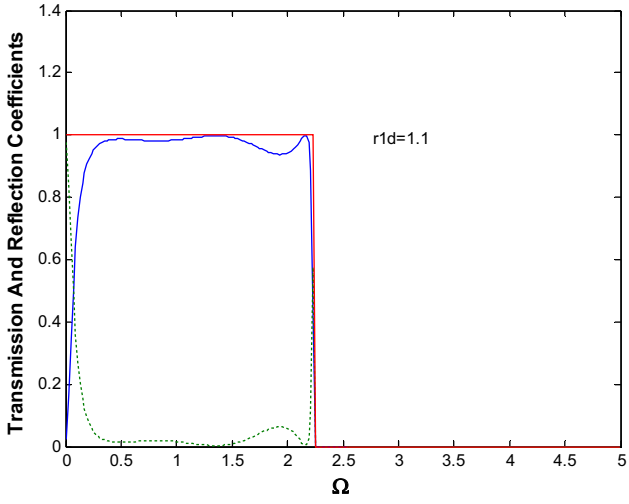

Figure 7: Transmissions and reflection coefficients in the case of hardening mode 1.

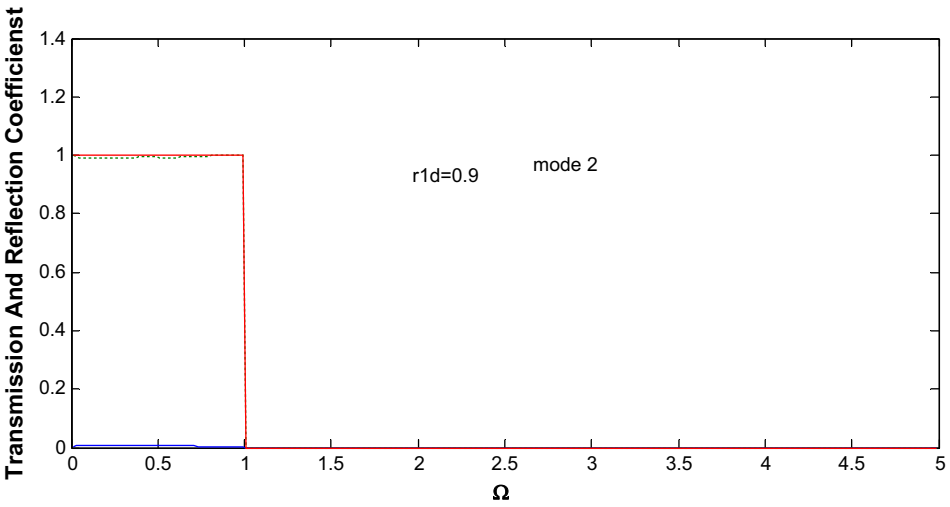

Figure 8: Transmission and reflection coefficients in the case of softening mode 2.

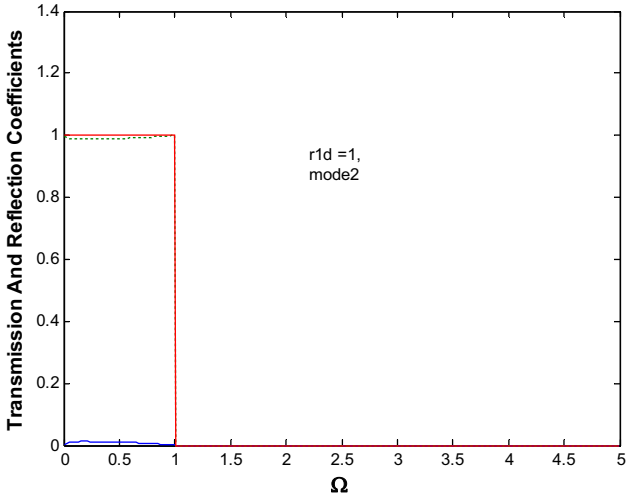

Figure 9: Transmission and reflection coefficients in the case of homogeneous mode 2.

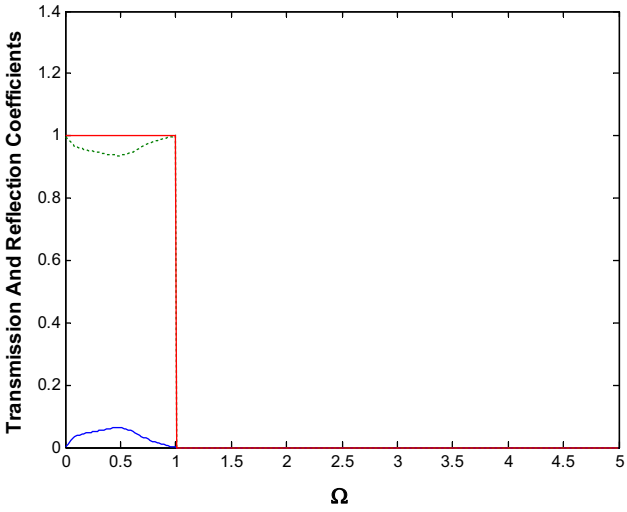

Figure 10: Transmission and reflection coefficients in the case of hardening mode 2.

as in the case of cuprates. However, contributions from other particles remain possible [34]. In metals, the movement of free electrons is predominant, while in the case of nonmetals, the vibration of the ions is the most important [35]. Thermal conductivity is therefore linked, on the one hand, to electrical conductivity (movement of charge carriers) and, on the other hand, to the very structure of the material (vibrations of atoms around their position of equilibrium). In fact, in a solid, the vibrations of atoms are not random and independent of each other but correspond to specific modes of vibration, which are also called "phonons." (We can make, for example, the analogy with a pendulum or a guitar string, whose vibration frequency is fixed.) These eigenmodes of vibration correspond to waves, which can propagate in the material if its structure is periodic (organized). This contribution will therefore be greater in a crystal that is ordered than in a glass that is disordered. In this study, the thermal conductivity was only considered due to the phonons. The phononic conductance was calculated as an essential parameter for the calculation of thermal conductivity. The waveguide conductance σ (Ω) (Bose–Einstein distribution) played an essential role in the whole analysis. For the net heat current, dQ_{12}, across the defect between the two ends of the waveguide, held between slightly different temperatures, $T + DT > T$, as follows:

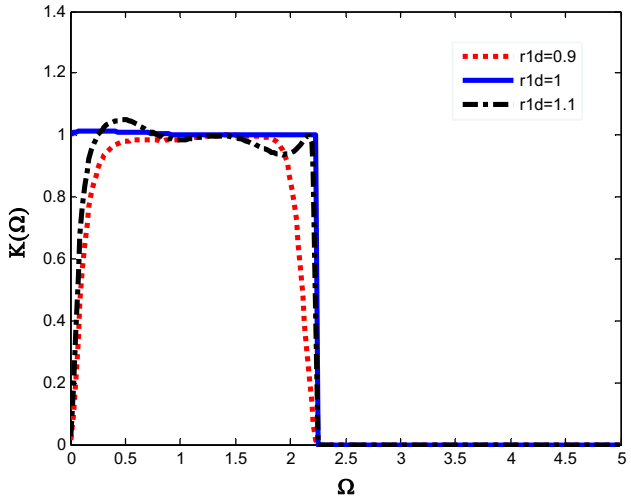

Figure 11: Phononic conductance or transmittance as function dimensionless Ω and elastic constant of the perturbed system.

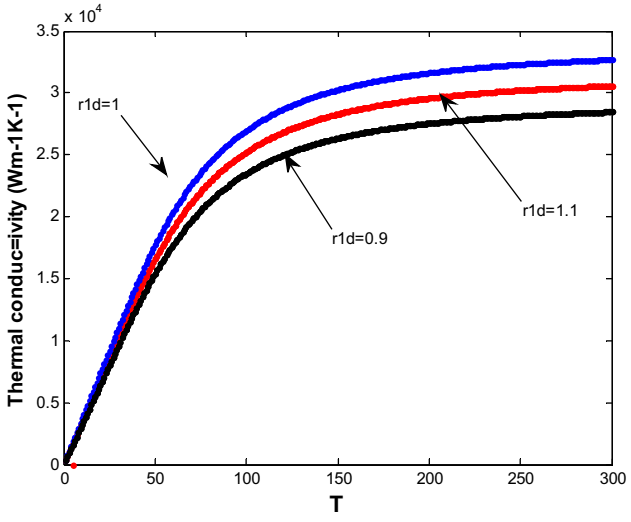

Figure 12: Thermal conductivity as function temperature and elastic constants near the defect.

$$\partial Q_{12} = \frac{1}{\ell}\sum_j \frac{1}{(2\pi)^2}\int \mathrm{d}q \upsilon_{gj}(q)\hbar\omega_j(q)\sigma_j(\omega_j, q) \times \frac{\partial n(T, \omega_j(q))}{\partial T}. \tag{14}$$

In general, electronic and phononic contributions ensured thermal conductivity rather than magnetic contributions in the case of ferromagnetic metals. In this study, the electronic contribution was investigated, and the heat was carried by the majority of charge carriers provided by the two modes. The thermal conductivities are presented in Figure 12 as a function of temperature and parameters of the behavior of the defect. The calculation curves showed that the heat transport contributions increased to reach a maximum value. Hence, this can be explained by the excitation of phonons. So, the thermal effect reduces the performance of electronic systems by thermal runaway.

5 Localized state at the behavior of the defect

The defects affect the various properties of the system and create localized states in its neighborhood that do not exist in the bulk. The localized states induced by the defect are directly linked to its nature, its geometry, and its modeling. So the number of localized branches is also linked to the number of sites that describe it. To determine the localized states in the vicinity of this inhomogeneity, we apply the dynamic equation of Newton to the minimum number of sites describing it, which gives us a defect matrix Md of dimension $(m \times n)$ rectangular for which we cannot determine the eigenstates and eigenvectors where the number of unknowns is greater than the number of equations. Therefore, a suitable method is necessary to solve the problem. There are several methods, including the mathing method on which our work is based. This one gives us a matching matrix of dimension $(n \times m)$ whose product with the defect matrix leads us to a square matrix, $Md \times Mr = Mp$ of dimension $(n \times n)$, whose eigenvalues give us the local states by [36–38]

$$\mathrm{Det}(\Omega I - Mp(rd_1, rd_2, \exp(i\phi_y)) = 0. \tag{15}$$

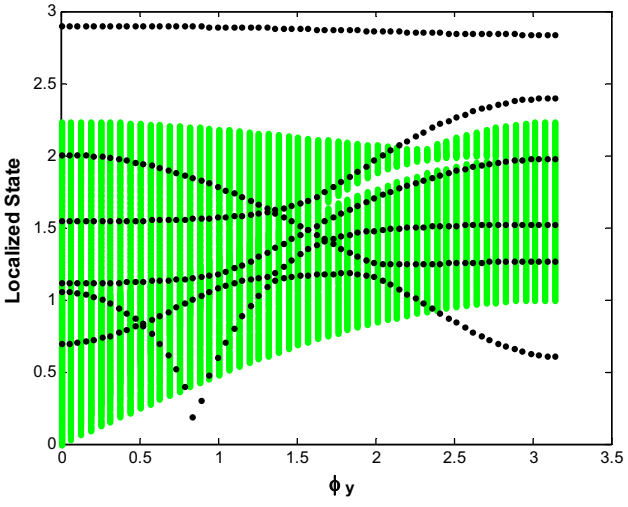

Figure 13: Branches of the localized state as function ϕ_y in BZ in the softening case.

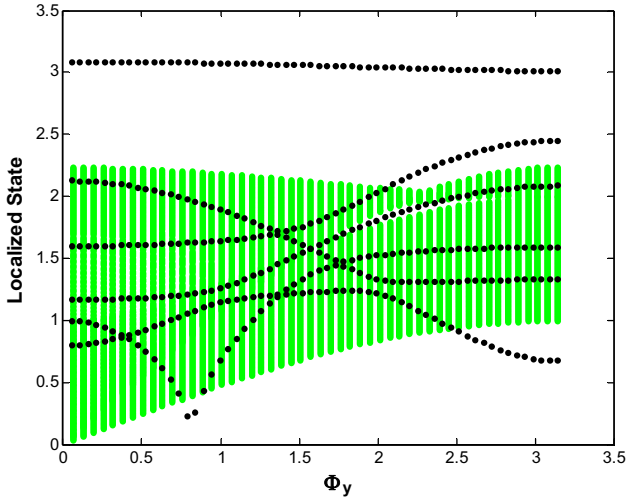

Figure 14: Branches of the localized state as function ϕ_y in BZ in the homogeneous case.

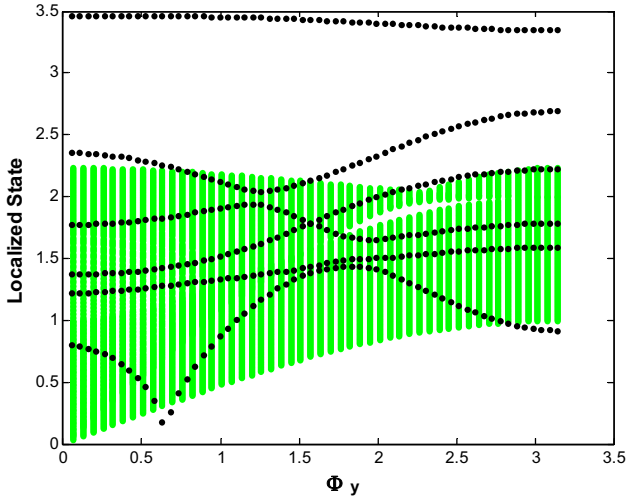

Figure 15: Branches of the localized state as function ϕ_y in BZ in the hardening case.

The number of branches is six in this case problem, and it is linked to the dimensions of the square matrix (6×6). The curves of localized branches are presented in Figures 13–15.

6 State density

The DOS is one of the basic quantities of any quantum system, and its determination is crucial in determining the physical properties of a system (e.g., heat capacity). Moreover, it is a capital quantity in experimental physics since it is directly measurable by inelastic neutron scattering.

As for electrons, it is possible to define a density of phononic states $G(\Omega)$, defined by the fact that the quantity is the number of states $G(\Omega)\mathrm{d}\Omega$ (modes) in the frequency $[\Omega,\ \Omega + \mathrm{d}\Omega]$ domain per unit cell of the material (system) studied. In the bulk, the DOS per site is strictly the same over all sites. In contrast, the sites at the defect of the present system have different atomic environments, and hence, they present different local densities of states (VLDOS) as a function of the sites. In this work, the most direct way to calculate the VLDOS in the vicinity of the defect is through a formalism based essentially on Green's functions and the phase-field matching theory matching formalism. The Green operator G, obtained from the square matrix (M_p) of the system, can be expressed in the following form [7,38–51]:

$$G(\phi_x, \phi_y, \Omega + i\varepsilon) = [(\Omega + i\varepsilon)I - Mp(rd_1, rd_2, \exp(i\phi_y))]^{-1}, \tag{16}$$

where Ω is the dimensionless frequency given by $\Omega^2 = \omega^2/\omega_0^2$, where ω_0 is a characteristic lattice frequency, ${\omega_0}^2 = k1/m$, where $k1$ is the force constant between first neighbors and m the mass of the atom. The spectral density matrix for a wave vector on the surface is given by the following relation:

$$\rho_{(\alpha,\beta)}^{(l,l')}(\varphi_x, \varphi_y, \Omega, Z) = \sum_m C_{\alpha m}^{l} \cdot C_{\beta m}^{l'} \cdot \delta(\Omega - \Omega_m) = \lim_{\varepsilon \to 0^+} [\mathrm{Im} G_{\alpha\beta}^{ll'}(\varphi_x, \varphi_y, \Omega + i\varepsilon)], \tag{17}$$

where l and l' represent two different sites, α and β represent two Cartesian directions, α is the component of the displacement u vector for the energy branch Ω_m, and ε is the distribution of Dirac (17).

The local density of state (LDOS) on the site l noted as $G_l(\Omega)$ corresponds to the sum of the trace of the spectral density matrices and can then be written as follows:

$$G_l(\Omega) = \sum_{l\alpha} \sum_{\varphi_x \varphi_y} \rho_{(\alpha,\alpha)}^{(l,l')}[\Omega, Z, \varphi_x, \varphi_y] = -\frac{1}{\pi} \sum_{l,\alpha} \sum_{\varphi_x, \varphi_y} \lim_{\varepsilon \to 0^+} [\mathrm{Im} G_{\alpha\alpha}^{ll}(\varphi_x, \varphi_y, \Omega + i\varepsilon)]. \tag{18}$$

7 Results and discussion

We can note, as a first remark, an exponential dependence of the amplitude of the evanescent phase factors

as a function of the dimensionless frequencies. Physically, this means that the higher the excitation frequency, the stronger the attenuation of the evanescent modes, characterized by the defect. We can also notice, on the other hand, that the phase factors $Z_i < 1$ with (i = 1,2) describe evanescent modes only when the frequency of the vibrational state is outside of a bandwidth, the width of which varies as a function of the ratio of the force constants $r2$ and of the angle of incidence Φ_y. For a frequency belonging to the pass band of the bulk phonons of the system, the phase factors have a modulus equal to one for the two modes and are propagating. To have a complete view of the dispersion relations, including both modes, the propagating and attenuated modes, it is interesting to represent on a 3D graph the trajectories traversed in the complex plane by the phase factors Z as a function of the normalized frequency Ω. For a fixed value of $r2$ = 0.25, we can therefore calculate the corresponding Z; and these solutions can be represented on (for the propagating modes) and inside (for the evanescent modes) a unit circle of the complex plane. Figure 4 presents such curves for the different modes 1 and 2 in the case of an incidence fy = 0 and $r2$ = 0.25.

We calculated the bulk phonon bandwidths for the ratio of force constants $r2$ = 0.25 in the case of a light mass defect (e = 0.3). The numerical calculations of equation (2) in the space $\{\Omega,\phi_y\}$ for different values of the ratio of the force constants in the vicinity of the defect, respectively, in softening, homogeneous and hard in the case of a light mass defect (e = 0.3), also show the existence of phonons located on the defect, the dispersion curves of which are superimposed with the pass bands of the volume phonons in Figure 10. Note that the number and the characteristics of these localized phonon dispersion curves strongly depend on the values of elastic parameters in the vicinity of the defect.

In Figure 13, the pass bands of the bulk modes are shown, as well as the dispersion curves of the localized phonons. We note that for a defect of light mass ratio (e = 0.3), when the ratio of the force constant r increases, it generates a spacing of the branches of the localized phonons. This situation is represented in Figures 14–15 in the case of an incidence ϕ_y = 0. They show the evolution of the frequency of the phonons located at the edge of the Brillouin zone as a function of the elastic parameters at the level of the defect called optical modes. We also notice that with the modification of the force constants, we come to situations where localized phonons are generated in the volume band window. Here too, the nature of the branches is linked with these parameters in the vicinity of the disturbed zone. In this work, we also calculated the transmission and reflection coefficients for the two modes 1 and 2 for the three cases of force constants in the vicinity of the softening, homogeneous, and hard defect. They are very sensitive to their variations, in particular the transmission, which decreases as a function of the increase in elastic constants in the vicinity of inhomogeneity. On the other hand, the resistance increases. The number of branches is directly related to the dimension of the square matrix, which is six in our case. In addition, the transmittance of the system, which is the sum of the transmissions of each mode, exhibits Fabry Perrot fluctuations due to the interference of the incident and reflected modes and also Fanon resonances due to the interaction of the modes located in the vicinity of the defect and those of the bulk. The thermal conductivity of the systems is directly linked to the phononic conductance of the system and the Bose–Einstein distribution. It is calculated for each mode and for all the modes. The contribution of each mode is additive. It was noticed that mode 2 is more energetic than the first, and it is calculated according to the temperature T. It also depends on the elastic parameters in the vicinity of the defect. They have a rough shape due to fluctuations in Fano resonances induced by the interaction of volume states and localized ones. In our case, the perturbed area contains six sites, for which the density was calculated based on the incident energy and parameters in the neighborhood of the defect. The works done before are also interesting results for different purposes [52–72].

8 Conclusion

In this study, the generic properties of phononic scattering at an integrated nanostructure in an inhomogeneous system model are studied by the matching technique in the harmonic approximation. The results show that the conductance of the system and of the reflection and transmission coefficients vary appreciably with the dimensionless frequencies and the atomic elastic defect parameters. At lower frequencies, the conductance starts with its maximal value, decreases with the increasing Ω, and vanishes at the Brillouin zone limit. These spectra may yield, from the theoretical and experimental points of view, useful information concerning the elastic parameters in the neighborhood of the defect and its specific nature. The conductance spectra can thus be used for identifying and investigating defects in specific nanostructures and then being used for their characterization. These findings can be verified in an easily realizable set of

experiments. Such systems can find some useful applications in the design of transducers and noise-destroying control devices (ultrasonic filters), whereas resonances are commonly used to build frequency filters. The results could also be useful for controlling thermal conductance artificially and the designing vibration-mode devices.

Acknowledgments: We would like to thank Ahmed Draia University for the working conditions made available to us.

Funding information: This research received no external funding.

Author contributions: The authors' contribution is equal.

Conflict of interest: The authors declare no conflict of interest.

Ethical approval: The conducted research is not related to either human or animal use.

Data availability statement: Data may be provided when it is requested from the corresponding author.

References

[1] Landauer R. Electrical transport in open and closed systems. Z Phys B Condens Matter. 1987;68(2–3):217–8.
[2] Büttiker M. Four-terminal phase-coherent conductance. Phys Rev Lett. 1986 Oct;57(14):1761–4.
[3] Szcześniak D, Khater A, Bąk Z, Szcześniak R, Ghantous MA. Quantum conductance of silicon-doped carbon wire nanojunctions. Nanoscale Res Lett. 2012 Nov;7(1):616.
[4] Szczésniak D, Khater A. Electronic conductance via atomic wires: a phase field matching theoryapproach. Eur Phys J B. 2012;85(6):1743.
[5] Khater A, Szczésniak D. A simple analytical model for electronic conductance in a one dimensional atomic chain across a defect. J Phys Conf Ser. 2011;289:01201.
[6] Amoudache S, Tigrine R, Khater A, Bourahla B. Interference effects in phonon scattering across a double atomic well. Eur Phys J B. 2010;73(3):405–12.
[7] Khater A, Auby N, Kechrakos D. Surface-surface phonon scattering by surface inhomogeneities. J Phys Condens Matter. 1992;4(14):3743–52.
[8] Belhadi M, Khater A. Spin wave modes and magnon scattering at surface nanostructure on 2d Heisenberg ferromagnets. Surf Rev Lett. 2004;11(1):99–109.
[9] Lai R, Kiselev SA, Sievers AJ. Intrinsic localized spin-wave resonances in ferromagnetic chains with nearest-and next-nearest-neighbor exchange interactions. Phys Rev B Condens Matter. 1997;56(9):5345–54.
[10] Bôni P, Roessli B, Gôrlitz D, Kôtzler J. Damping of spin waves and singularity of the longitudinal modes in the dipolar critical regime of the Heisenberg ferromagnet EuS. Phys Rev B Condens Matter. 2002;65(14):144434.
[11] Allen RE, Alldredge GP, de Wette FW. Studies of vibrational surface modes. I. general formulation. Phys Rev, B, Solid State. 1971;4(6):1648–60.
[12] Lockj AP, Toennies G. Witte, surface phonons of stepped metal surfaces. J Electron Spectrosc Relat Phenom. 1990;54–55:309–16.
[13] Niu LD, Gaspar J, Sibener SJ. Phonons localized at step edges: A route to understanding forces at extended surface defects. Sci New Ser. 1995;268(5212):847–50. https://Www.Jstor.Org/Stable/2887963
[14] Knipp P. Phonons on stepped surfaces. Phys Rev B. Published 15 March 1991;43:6908–23. doi: 10.1103/PhysRevB.43.6908.
[15] Belhadi M, Chadli R, Khater A, Abou Ghantous M. Spin dynamics across an inhomogeneous atomic boundary separating ultrathin Heisenberg ferromagnetic films. Eur Phys J Appl Phys. 2007;37(1):25–31.
[16] Dobrzynski L. Interface response theory of discrete composite systems. Surf Sci Rep. 1986;6(3):119–57.
[17] Masri P, Allan G, Dobrzynski L. Perturbations de quelques propriétés vibrationnelles des surfaces cristallines par les marches. J Phys (Paris). 1972;33(1):85–93.
[18] Landauer R. Spatial variation of currents and fields due to localized scatterers in metallic conduction. IBM J Res Dev. 1957;1(3):223–31.
[19] Landauer R. Electrical resistance of disordered one-dimensional lattices. Philos Mag. 1970;21(172):863–7.
[20] Büttiker M. Four-terminal phase-coherent conductance. phys rev lett. 1986;57:1761–4. doi: 10.1103/PhysRevLett.57.1761
[21] Lai R, Kiselev SA, Sievers AJ. Intrinsic localized spin-wave resonances in ferromagnetic chains with nearest- and next-nearest-neighbor exchange interactions. Phys Rev B Condens Matter. 1997;56(9):5345–54.
[22] Binnig G, Rohrer H, Gerber C, Weibel E. Surface studies by scanning tunneling microscopy. Phys Rev Lett. 1982;49(1):57–61.
[23] Fukuma T, Kobayashi K, Matsushige K, Yamada H. True atomiC resolution in liquid by frequency-modulation atomic force microscopy. Appl Phys Lett. 2005;87(3):34101.
[24] Armand G. Generating lattice Green's functions. Phys Rev B. 1976;14(6):2218–28.
[25] Armand G. Détermination des grandeurs liées aux modes de vibrations d'un cristal. spectre de fréquence. Densité spectrale d'un atome de surface et déplacements corrélés moyens. J Phys (Paris). 1977;38(8):989–1005.
[26] Armand G, Masri P. Localized surface modes and resonances for vicinal surfaces: The (117). Surf Sci. 1983;130(1):89–123.
[27] Garcia-Moliner F. The physics of surface green function matching. Ann Phys (Paris). 1977;2:179–200.
[28] Allen RA. A general green function method for calculating electronic structure and vibrational modes at surfaces. Surf Sci. 1978;76(1):91–101.
[29] Treglia G, Desjonqueres MC. Bulk and surface vibrational and thermodynamical properties of fcc transition and noble

metals: a systematic study by the continued fraction technique. J Phys (Paris). 1985;46(6):987–1000.
[30] Liu Y, Jiang P, Zhang D, Zhou G. 3D-feature-based structure design for silicon fabrication of micro devices. Microsyst Technol. 2007;13(7):701–14.
[31] Teo BK, Sun XH. From top-down to bottom-up to hybrid nanotechnologies: road to nanodevices. J Clust Sci. 2006;17(4):529–40. doi: 10.1007/s10876-006-0086-5.
[32] Tseng AA, Notargiacomo A, Chen TP. Nanofabrication by scanning probe microscope lithography: A review. J Vac Sci Technol. 2005;B23:877–94.
[33] Hansma PK, Tersoff J. Scanning tunneling microscopy. J Appl Phys. 1987;61:R1–R24.
[34] Slater JC. Quantum Theory of Molecules and Solids. New York, London: M. C. Graw-Hill; 1965.
[35] Maradudin AA, Melangalis J. Phys Rev A. 1967;133:1118.
[36] Grimech H, Khater A. Calculation of the spectral densities of the surface alloy system (Pt_cCu_{1-c1}/Cu(100). 1995;323(3):198–206.
[37] Grimech H, Khater A. Mean surface phonon dispersion curves for low index fcc $(A_c/B_{1-c})_1B(klm)$ surface alloys. Surf Sci. 1995;341(3):227–40.
[38] Virlouvet A, Grimech H, Khater A, Pennec Y, Maschke K. Dynamical properties of an isolated step. J Phys Condens Matter. 1996;8(41):7589–603.
[39] Feuchtwang TE. Dynamics of a semi-infinite crystal lattice in a quasiharmonic approximation. II. The normal-mode analysis of a semi-infinite lattice. Phys Rev. 1967;155(3):731–44.
[40] Szeftel J, Khater A. Calculation of surface phonons and resonances: The matching procedure revisited. J Phys C Solid State Phys. 1987;20(29):4725–36.
[41] Szeftel J, Khater A, Mila FS, D'Addatoet N, Auby J. Calculation of surface phonon dispersion on Ni(100) and Ni(100)+c(2×2) along the (010) direction by means of the matching procedure. II. Phys C Solid State Phys. 1988;21:2113–36.
[42] Khater A, Czaja W. Impurity-impurity interaction mediated by coherent phonons. Phys B. 1990;167(1):33–9.
[43] Belhadi M, Rafil O, Tigrine R, Khater A, Hardy J, Virlouvet A, et al. Klaus maschke the scattering and transmission of elastic waves in quasi-two-dimensional planar waveguides with linear defect boundaries. Eur Phys J B. 2000 May;15(3):435.
[44] Felly A, Gagel F, Maschke K, Virlouvet A, Khater A. Scattering of vibrational waves in perturbed quasi-one-dimensional multichannel waveguides. Phys Rev B Condens Matter. 1997;55:1707–17.
[45] Fellay A. Rapport Master d'ingénieur physicien. Ecole Polytechnique Fédérale de Lausanne; 1996.
[46] Landauer R. Conductance determined by transmission: probes and quantised constriction resistance. J Phys Condens Matter. 1989;1(43):8099–110.
[47] Khater A, Auby N, Wallis RF. Some dynamical properties of the alloy disordered chain on a semi-infinite solid square lattice. Surf Sci. 1989;217(3):563–72.
[48] Belhadi M, Rafil O, Tigrine R, Khater A, Hardy J, Virlouvet A, et al. The scattering and transmission of elastic waves in quasi-two-dimensional planar waveguides with linear defect boundaries. Eur Phys J B. 2000;15(3):435–43.
[49] Khater A, Belhadi M, Abou Ghantous MM. Phonons heat transport at an atomic well boundary in ultrathin solid films. Eur Phys J B. 2011;80(3):363–9.
[50] Zerirgui D, Tigrine R, Bourahla B. Dynamic properties of integrated nanostructure on metallic surface. J Appl Phys. 2012;111(4):044907.
[51] Dobrzynski L, Mills DL. Vibrational properties of an adsorbed surface layer on a simple model crystal. J Phys Chem Solids. 1969;30(5):1043–58.
[52] Ural A, Kilimci ZH. The prediction of chiral metamaterial resonance using convolutional neural networks and conventional machine learning algorithms. Int J Comput Exp Sci Eng. 2021;7(3):156–63.
[53] Sarihan M. Simulation of gamma-ray shielding properties for materials of medical interest. Open Chem. 2022;20(1):81–7.
[54] Demir N, Kıvrak A, Üstün M, Cesur A, Boztosun I. Experimental study for the energy levels of europium by the clinic LINAC. Int J Comput Exp Sci Eng. 2017;3(1):47–9.
[55] Iskender Akkurt I. Effective atomic and electron numbers of some steels at different energies. Ann Nucl En. 2009;36(11–12):1702–5. doi: 10.1016/j.anucene.2009.09.005.
[56] Caymaz T, Çalışkan S, Botsalı AR. Evaluation of ergonomic conditions using fuzzy logic in a metal processing plant. Int J Comput Exp Sci Eng. 2022;8(1):19–24.
[57] Akkurt I. Effective atomic numbers for Fe–Mn alloy using transmission experiment. Chin Phys Lett. 2007;24(10):2812–4.
[58] ALMisned G, Sen Baykal D, Kilic G, Susoy G, Zakaly HMH, Ene A, et al. Assessment of the usability conditions of Sb2O3-PbO-B2O3 glasses for shielding purposes in some medical radioisotope and a wide gamma-ray energy spectrum. Appl Rheol. 2022;32(1):178–89.
[59] Arbouz H. Modeling of a tandem solar cell structure based on CZTS and CZTSe absorber materials. Int J Comput Exp Sci Eng. 2022;8(1):14–8.
[60] Çilli A, Beken M, Kurt N. Determination of theoretical fracture criteria of layered elastic composite material by ANFIS method from artificial intelligence. Int J Comput Exp Sci Eng. 2022;8(2):32–9.
[61] Almisned G, Sen Baykal D, Susoy G, Kilic G, Zakaly HMH, Ene A, et al. Determination of gamma-ray transmission factors of WO3–TeO2–B2O3 glasses using MCPX Monte Carlo code for shielding and protection purposes. Appl Rheol. 2022;32(1):166–77. doi: 10.1515/arh-2022-0132.
[62] Waheed F, İmamoğlu M, Karpuz N, Ovalıoğlu H. Simulation of neutrons shielding properties for some medical materials. Int J Comput Exp Sci Eng. 2022;8(1):5–8.
[63] Safiddine S, Amokrane K, Debieb F, Soualhi H, Benabed B, Kadri E. How quarry waste limestone filler affects the rheological behavior of cement-based materials. Appl Rheol. 2021;31(1):63–75.
[64] Şen Baykal D, Tekin H, Çakırlı Mutlu R. An investigation on radiation shielding properties of borosilicate glass systems. Int J Comput Exp Sci Eng. 2021;7(2):99–108.
[65] Tan T, Zhao Y, Zhao X, Chang L, Ren S. Mechanical properties of sandstone under hydro-mechanical coupling. Appl Rheol. 2022;32(1):8–21.
[66] Tekin HO, Cavli B, Altunsoy EE, Tugba Manici T, Ozturk C, Karakas HK. An investigation on radiation protection and shielding properties of 16 slice computed tomography (CT) facilities. Int J Comput Exp Sci Eng. 2018;4–2:37–40. doi: 10.22399/ijcesen.408231

[67] Karaali R, Keven A. Evaluation of four different cogeneration cycles by using some criteria. Appl Rheol. 2022;32(1):122–37.
[68] Bekir O. Gamma-ray shielding properties of Nd2O3 added Iron-Boron-Phosphate based composites. Open Chem. 2022;20(1):237–43.
[69] Salima B, Seloua D, Djamel F, Samir M. Structure of pumpkin pectin and its effect on its technological properties. Appl Rheol. 2022;32(1):34–55.
[70] Arslankaya S, Çelik MT. Prediction of heart attack using fuzzy logic method and determination of factors affecting heart attacks. Int J Comput Exp Sci Eng. 2021;7(1):1–8.
[71] Ayhan E. Structural, physical, and mechanical properties of the TiO_2 added hydroxyapatite composites. Open Chem. 2022;20(1):272–6.
[72] Özseven A. Assessment of using electronic portal imaging device for analysing bolus material utilised in radiation therapy. Open Chem. 2022;20(1):61–8.